International Journal of Thermal Sciences 168 (2021) 107049

Contents lists available at ScienceDirect

International Journal of Thermal Sciences

journal homepage: www.elsevier.com/locate/ijts

Computational compensation of systematic errors accompanying non-equilibrium thermocouple measurements

Václav Kočí [a,*], Jan Kočí [a], Jiří Maděra [a], Jiří Litoš [b], Vojtěch Pommer [a], Lenka Scheinherrová [a], Robert Černý [a]

[a] Department of Materials Engineering and Chemistry, Faculty of Civil Engineering, Czech Technical University in Prague, Thákurova 7, 166 29, Prague 6, Czech Republic
[b] Experimental Center, Faculty of Civil Engineering, Czech Technical University in Prague, Thákurova 7, 166 29, Prague 6, Czech Republic

ARTICLE INFO

Keywords:
Thermocouple
High temperature
Thermal conductivity
Systematic errors
Computational modeling

ABSTRACT

Application of thermocouple sets of various complexity as temperature sensors in porous materials can be accompanied with systematic errors related to the very high differences between the thermal conductivities of thermocouple forming metals and measured samples. Since the higher measurement uncertainties can then make some presumed utilizations of measured temperature fields questionable, this paper introduces an approach which can overcome this drawback. Using a computational model, it is able to separate parameters of particular constituents of the sample-thermocouple system that helps to filter out the systematic errors by means of extracting the pure material parameters. The applicability of the approach is demonstrated on a one-sided high-temperature heating experiment, in which the temperature field in a sample is monitored and subsequently used for the determination of thermal conductivity. The effect of the computational compensation procedure is found to be very significant. The up to 64 °C temperature differences between the raw data and corrected values can cause systematic thermal conductivity errors of up to 46%. Depending on temperature, the corrected thermal conductivity is then by up to 0.89 W m^{-1} K^{-1} lower.

1. Introduction

Thermoelectric properties of metal wires junctions have been known since the 19th century when the early history of thermocouples is dated. Since the first research and discoveries made by Seebeck, Oersted, Ampére, Becquerel and others [1], the thermocouples made a substantial progress and became one of the key methods for measurement of temperature and temperature-related parameters in most scientific disciplines. The principle of a thermocouple is very simple: it produces a temperature-dependent voltage as a result of the thermoelectric effect. This voltage can be subsequently measured and interpreted to express the temperature. High accuracy, fast thermal response, wide operating temperature range, low costs, and high reliability belong among the most essential properties that have contributed to a broad utilization of thermocouples in the form of various temperature sensors [2,3].

In the field of building materials engineering, thermocouples are widely used for monitoring of thermal performance of materials, whole buildings, or their parts. Al-Naghi et al. [4] used thermocouples to perform a field test aimed at the investigation of thermal performance of walls made of autoclaved aerated concrete in order to make a comparison with a wall made of hollow concrete block. Combining the thermocouples with other equipment, such as weather stations, infrared cameras, heat flux meters or relative humidity sensors, they were able to obtain a detailed performance comparison of the walls studied. Ding et al. [5] used K-type thermocouples to monitor temperature field inside carbon fiber reinforced plastic composites to validate their three dimensional thermal model for the calculation of temperature distribution when irradiated by a laser. The same type of thermocouples was used also by Bendouma et al. [6] who investigated hygric and thermal performance of various thermal insulation systems, both contact and ventilated, to assess risks of water vapor condensation. The nature of thermocouples, i.e. a combination of various metals, predisposes them to be used for high temperature measurements as well. Recording temperatures up to 1000 °C, Drozdzol [7] mounted a set of thermocouples to a chimney and an adjacent wooden construction that the chimney went through to evaluate fire risks in such a type of materials combination. During their experiment aimed at the measurement of temperature distributions in an oil-fired tunnel furnace, Lou et al. [8]

* Corresponding author.
E-mail address: vaclav.koci@fsv.cvut.cz (V. Kočí).

https://doi.org/10.1016/j.ijthermalsci.2021.107049
Received 24 November 2020; Received in revised form 20 April 2021; Accepted 30 April 2021

used thermocouples for temperature monitoring to avoid overheating of a refractory wall that might occur at 1260 °C. Arends et al. [9] attached a set of thermocouples in a wooden sample exposed to one-sided heating to record temperature during the experiment and couple it with the moisture transport.

Besides a simple monitoring of thermal performance, the thermocouples can be used for gathering data that is further processed and evaluated to obtain various thermal parameters of materials investigated. The determination of the thermal conductivity [10,11] or specific heat capacity [12] as a function of temperature can be mentioned as examples in that respect, being based on measuring temperature fields in a material sample and a subsequent solution of the inverse heat conduction problem.

Since the thermocouples are made of metals, their thermal conductivity is much higher compared to porous building materials. It means, their insertion in a sample might go along with a substantial deformation of the temperature field and thus to a distortion of data provided, which was proved, e.g., by Cherepanov et al. [13] in their work aiming at the identification of factors affecting thermocouple measurements. The consecutive processing of data recorded, logically, has to reflect this distortion as the results obtained are affected by systematic errors. This phenomena, especially in case of building materials engineering, can be considered as the biggest shortage of this method, which is very reliable in other cases. Kong et al. [14], for instance, demonstrated that the temperature field determined using thermocouples might exhibit a difference of more than 20 °C when compared with the reconstructed temperature fields obtained using acoustic tomography and processed by various models. Looking for other techniques for determination of internal temperature fields, several researchers proposed ultrasonic methods. Ihara et al. [15] demonstrated their applicability on a steel plate. Unfortunately, as steel has similar thermal conductivity like the thermocouple wires, a conclusion about their use in porous building materials cannot be made. Moreover, they used thermocouple data itself for a validation of the method proposed. An influence of a thermocouple on heat flux through a sample was mentioned by Wen et al. [16]. Depending on the thermocouple position, they reported differences in heat flux vs. time functions when compared to results obtained using the smoothing technique proposed.

Despite the aforementioned shortages, the application of thermocouples in building materials research is still very advantageous. The destructive nature of the testing procedure does not play a significant role here as the thermocouples are purposely built in samples that are produced primarily for an experimental investigation. Additionally, the possibility for their insertion without drilling, e.g. in case of materials that undergo a hardening process, represents another argument against the thermocouples' disadvantages. The problem of the temperature field distortion, originating from different thermal conductivities of porous materials and metals, remains the most important issue that has to be dealt with. This issue, however, concerns also other methods for determination of thermal conductivity, which has been, among others, pointed out by Nabil and Khodadadi [17], who analyzed a transient hot-wire technique. It is therefore believed that the proposed technique is worth investigating instead of searching for other methods, such as ultrasound or acoustic tomography, that could possibly replace the thermocouples.

This paper introduces a new approach for reduction of systematic errors that accompany an experimental determination of temperature fields in porous samples using thermocouples, which also includes the subsequent data processing. The applicability of this approach is demonstrated on a porous cement based sample that is exposed to high temperatures during a one-sided heating experiment. The temperature-dependent thermal conductivity of the sample is evaluated on the basis of the measurement of temperature field and subsequent solution of the inverse heat transport problem. The thermal conductivity calculated on the raw-experimental-data basis is compared with that obtained by means of the temperature distribution corrected using a three-dimensional computational modeling of the heat transport. Finally, the contribution of this approach to the systematic errors reduction is evaluated.

2. Materials and methods

2.1. Samples

The samples studied had dimensions of 70 mm × 70 mm × 140 mm. They were made of a hydraulic binder with a high content of alumina (Blaine fineness 3700–4500 $cm^2\ g^{-1}$, chemical constituents by XRF: Al_2O_3 = 68.5%, CaO = 31.0%, SiO_2 = 0.8%, Fe_2O_3 = 0.4%), fireclay aggregates (chemical constituents by XRF: SiO_2 = 54.0%, Al_2O_3 = 41.7%, Fe_2O_3 = 1.3%, TiO_2 = 1.5%) of various fractions, and water. The composition of the mixture is summarized in Table 1. After the samples had been cast, they were cured for 28 days.

2.2. System of thermocouples

A chromel-alumel (K-type) thermocouple system was manually prepared to be built in the sample to monitor temperature distribution during a one-sided heating experiment. The designed set of thermocouples was made of one unsheathed chromel core wire (d = 1.2 mm) and twelve unsheathed alumel side wires (d = 1.2 mm) attached to it in different positions using a silver solder. Therefore, it was able to measure temperatures up to 1260 °C in twelve different positions across the sample investigated. Since the wires are without coating, the thermocouple is able to respond to temperature changes very quickly (t_{resp} < 1.0 s). Fig. 1 shows the positions of the particular wires, together with the computational representation of the set. The sample with built-in thermocouples is depicted in Fig. 2. During the casting process, the ends of thermocouple wires outside the mold were fixed using clips to ensure the spatial stability before the mixture setting. This was important especially when the sample was compacted by vibrating to ensure a full contact of the wires with the body of the sample.

It should be noted that the thermocouple set depicted in Fig. 1 was prepared "ad hoc" because such a product is not available at the commercial market. Therefore, it does not fully conform with the standardized thermocouple sensors. The multiple wires arrangement or their thickness can be mentioned in particular. This corresponds to a fact, that the thermocouple set is primarily designed to be built in a cement-based sample within the casting procedure, so that the additional drilling due to the sensors insertion could be omitted. The increased thickness of the wires is therefore essential to avoid their spatial instability, deformation, or even breaking during the casting procedure. On the other hand, it goes along with an increased thermal bridging which might be a source of additional measurement errors. Compensatory techniques should therefore complement the measurement as it will be described later in this paper.

Data provided by a K-type thermocouple are generally considered very precise and consistent [18]. However, as this thermocouple set has a specific structure of a multi-thermocouple and it was prepared in laboratory conditions, it does not represent a standard piece of an instrument. Therefore, a control calibration procedure was performed prior to the experiments, being supposed to verify the thermocouple applicability and functionality. Such a procedure was also supposed to exclude any malfunctions, that may exist due to a presence of inclusions,

Table 1
The composition of the mixture for the samples preparation.

Constituent	Dosage [$kg \cdot m^{-3}$]
High alumina cement	500.0
Fireclay aggregates 0/0.5	770.0
Fireclay aggregates 0.5/1	730.0
Water	337.5

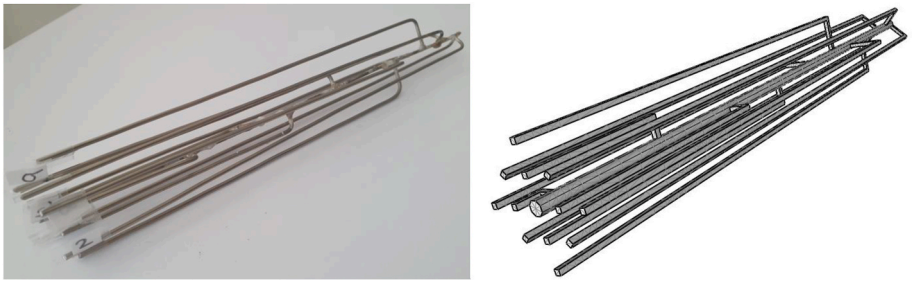

Fig. 1. The thermocouple set used in the experiments including its computational representation.

Fig. 2. The reference sample and the sample with built-in thermocouples.

as the soldering of the side wires was carried out in standard (non-protective) environment. Within this calibration, the whole sample was placed in the furnace, being exposed to selected constant temperatures for time periods long enough to reach a steady state. The steady-state values of thermoelectric voltage recorded on particular thermocouples were then compared with the temperature in the furnace, yielding a voltage/temperature conversion factor. Four different temperatures were selected for the calibration procedure, and the obtained conversion function was compared with the standard function for K-type thermocouples [19]. Because of the limited temperature resistance of the connecting wires between the thermocouple set and the data logger, all the temperatures must have been lower than 260 °C. Moreover, it has been reported that an application of K-type thermocouple above 200 °C might be destructive [18] due to some irreversible changes that might occur (oxidation in particular). Although it does not mean that the thermocouple cannot be used anymore, the measurement errors can be higher with an increasing number of applications. This fact represented an additional justifying argument for the calibration at lower temperatures. The other values were then extrapolated using a linear function which was in an agreement with the standard calibration function of K-type thermocouples in the range of 20–1100 °C [19].

2.3. One-sided heating experiment

In the one-sided heating experiment the temperature field was recorded as a function of time using the thermocouple set built in the sample until the steady state was reached. The obtained data provided thus information on both transient and steady state heat transfer. The transient temperature profiles were then processed by means of solving the inverse problem of heat conduction to determine thermal conductivity as a function of temperature, $\lambda_{exp}(T)$. The methodology was described in detail by Černý and Vejmelková [10]. Unfortunately, there was a good reason to believe that the raw temperature data were not accurate enough. The high difference between the supposed thermal conductivity of the porous sample and the thermocouple wires was, apparently, a source of systematic errors which deformed the temperature field. Furthermore, the assumption of the unidirectional heat transfer mode adopted in the inverse heat transfer problem solution [10] is impossible to ensure practically, even if the experimental setup is designed to fulfill these conditions (one-sided heating, shape ratio of the sample, side walls insulations, etc.) as much as possible. Therefore, a computational technique (described in Sections 2.4 and 2.5) was used to correct the uncertainties in temperature measurement.

The experiments were performed using a laboratory furnace (type 1013 L, made by Clasic CZ) of which door had been modified to accommodate the sample. Adding an extra insulation layer, the thickness of the door was adjusted to 140 mm which corresponded to the length of the sample (see Fig. 3a). This was one of the essential factors that conditioned the approximation to the one-dimensional heat transfer mode throughout the sample. However, the real transfer mode will always be multidimensional, especially when the thermocouple arrangement is spatial. However, these discrepancies can be accommodated and treated within the computational modeling aimed at the reduction of systematic errors.

Once the furnace temperature reached 1100 °C, the solid door was replaced by that with the sample, so that the heat transfer was initiated. The particular wires of the thermocouples were connected to a data logger MS6D made by Comet (see Fig. 3b) and the thermoelectric voltage values were continuously recorded, being converted to temperature values. The scheme of the thermocouple positions and boundary conditions is depicted in Fig. 4. The heat transfer coefficient, $\alpha_e = 6.47\ W\ m^{-2}\ K^{-1}$, used in the calculations on the exterior side was taken from a previous research [20]. On the other hand, the heat transfer coefficient in the furnace is very specific as it takes several heat transfer modes into consideration, the radiation in particular. Therefore, a precise determination of this coefficient was performed separately by means of a detailed analysis of surface temperature evolution. The initial temperature of the sample corresponded to the temperature in the laboratory (25 °C).

2.4. Computational modeling of heat transfer

A 3-D computational modeling procedure was used to calculate the temperature distribution across the sample during the experiment. Being formed of 35,599 nodes and 190,381 tetrahedral elements to accommodate all the tiny details of the thermocouples, the model was supposed to represent an exact replica of the experiment, including the initial and boundary conditions, as described in Section 2.3. The computational mesh with a part of the sample being cut off for a better illustration is depicted in Fig. 5.

The distribution of temperature inside the sample-thermocouple system was modeled using the three-dimensional heat transport equation

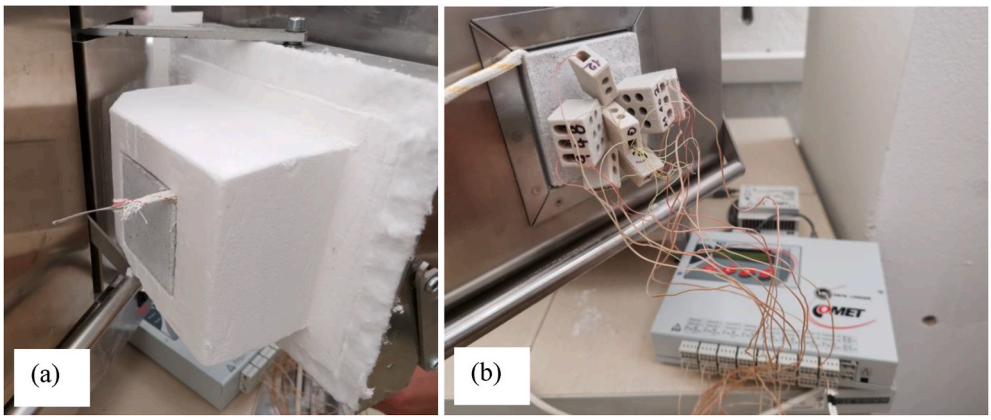

Fig. 3. (a) The modified furnace door with the sample accommodated, (b) the thermocouple-data logger connection.

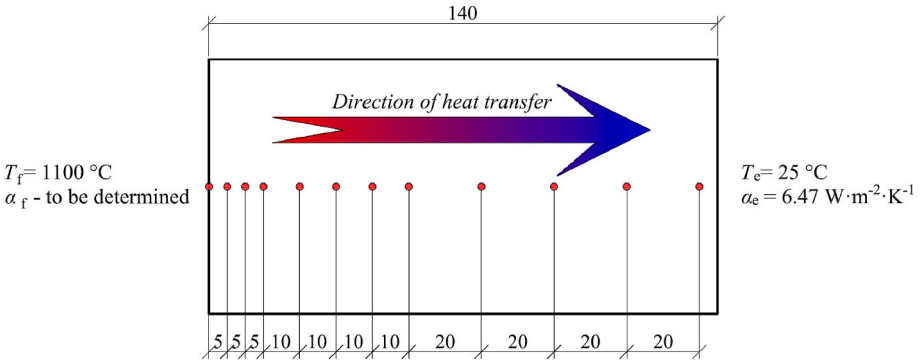

Fig. 4. Scheme of the one-sided heating experiment including the positions of temperature sensors.

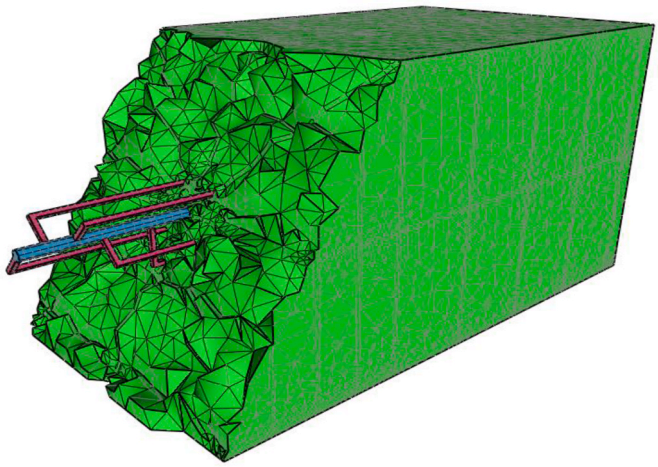

Fig. 5. Computational model of the sample with built-in thermocouples.

$$\rho_i c_i \frac{\partial T}{\partial t} = \mathrm{div}(\lambda_i \cdot \mathrm{grad} T) = \frac{\partial}{\partial x}\left(\lambda_i \frac{\partial T}{\partial x}\right) + \frac{\partial}{\partial y}\left(\lambda_i \frac{\partial T}{\partial y}\right) + \frac{\partial}{\partial z}\left(\lambda_i \frac{\partial T}{\partial z}\right). \quad (1)$$

where $\rho_i = \rho_i(T)$ [kg·m^{-3}] is the bulk density as a function of temperature, $c_i = c_i(T)$ [J·kg^{-1}·K^{-1}] the specific heat capacity as a function of temperature, $T = T(x, y, z, t)$ [K] the temperature as a function of space and time, t [s] the time, and $\lambda_i = \lambda_i(T)$ [W·m^{-1}·K^{-1}] the thermal conductivity as a function of temperature. The subscript i refers to particular components of the sample-thermocouple system. Since the sample has a porous structure, other heat transfer modes besides conduction are to be taken into account as well. Its thermal conductivity must be therefore understood as an effective value that considers all these modes.

The heat transport equation (1) was then solved numerically using the finite element method. The material parameters required for the modeling are summarized in Table 2 [21] and Figs. 6 and 7. Specific heat capacity of the sample was determined using the differential scanning calorimetry (Labsys™ Evo DTA/DSC made by SETARAM Inc.). Based on the thermogravimetric method, the same device was used also to calculate bulk density as a function of temperature.

2.5. Principles of experimental data correction

The determination of the effective thermal conductivity, $\lambda_{exp}(T)$, based on a one-sided heating experiment involves processing of the experimentally measured temperature field by a relatively simple computational technique [10]. Therefore, it might seem very advantageous. It is though important to realize, that the thermocouple-based measurement technique distorts the temperature field due to the metal wires presence, so the calculated data based on the distorted temperature field contains a systematic error. In order to overcome this serious drawback of the, in other respects, reliable method, a 3-D computational model of the experiment was designed to perform an inverse analysis of the distorted temperature field with respect to the particular materials in

Table 2
Material properties.

Material	Bulk density [kg m^{-3}]	Thermal conductivity [W m^{-1} K^{-1}]	Specific heat capacity [J kg^{-1} K^{-1}]
Chromel	8610	see Fig. 6	235–510
Alumel	8500		235–510
Sample	see Fig. 7	the objective of the modeling procedure	see Fig. 7

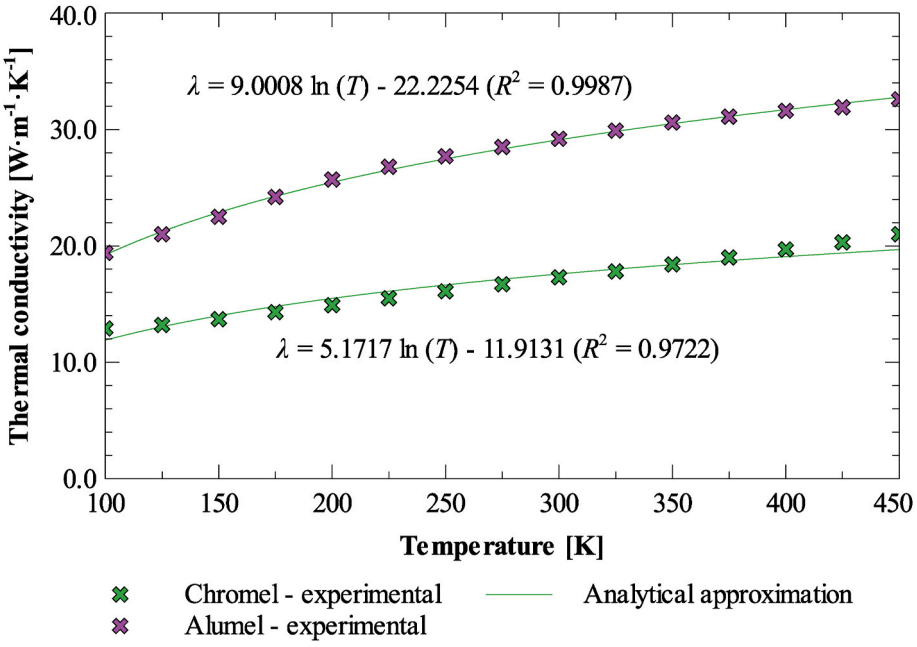

Fig. 6. Thermal conductivity of chromel and alumel wires as functions of temperature.

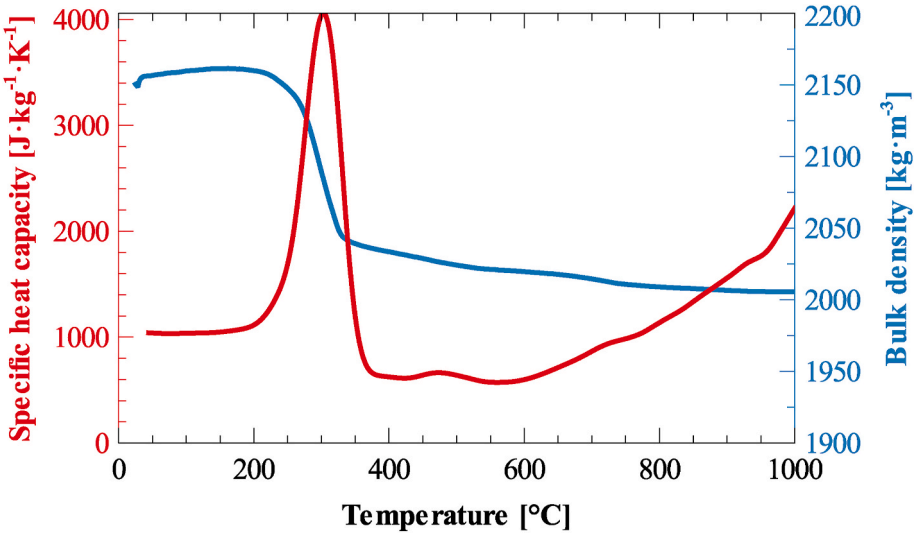

Fig. 7. Specific heat capacity and bulk density of the sample as functions of temperature.

the sample-thermocouple system.

The main objective of the modeling procedure is to exploit the inverse analysis to estimate such a thermal conductivity vs. temperature function, $\lambda_s(T)$, of the sample tested, that in an interaction with the metal wires provides the same temperature distribution as the experimental measurement. Since the computational model is supposed to be an exact replica of the experiment, i.e., it contains the sample with the built-in thermocouple set of known material parameters, it is able to deform the temperature field in the same way like it is deformed in the real experiment. However, the crucial advantage of the model is its ability to distinguish between the particular materials of the sample-thermocouple system, so it can extract the thermal conductivity of the pure sample, $\lambda_s(T)$. Such a thermal conductivity function found by the modeling procedure can be then understood as more accurate as the systematic errors are substantially reduced.

Once the thermal conductivity function, $\lambda_s(T)$, is determined computationally, it is compared with the $\lambda_{exp}(T)$ function, obtained using the processing of the raw experimental data. In this way, the contribution of the model from the point of view of the accuracy improvement and systematic errors reduction can be quantified.

To find the thermal conductivity function, $\lambda_s(T)$, computationally within the inverse analysis, it is highly advantageous to use an advanced seeking technique to avoid trial-and-error procedures which would be very time demanding. The genetic algorithms [22] were therefore exploited for this purpose. This technique is very versatile and has been successfully involved in various tasks in the field of building materials engineering [23–26]. It adopts processes related to an evolution of living species and transfers them to the artificial intelligence theory to find the best solution. The genetic algorithm GRADE [27] was used for this purpose, which was developed at the Department of Mechanics, Faculty of Civil Engineering, Czech Technical University in Prague to solve identification and optimization problems in the field of structural design and mechanics [28,29]. The source code of the algorithm was slightly modified during implementation to be capable of solving heat and mass

transfer problems. It works with real-coded vectors that represent candidate solutions to the optimization problem, where the vector dimension corresponds to the number of optimized variables. The algorithm uses three genetic operators, i.e., mutation, cross-over, and selection, which are mathematically defined as vector operations. The detailed description of these operators is given in the documentation [27].

Assuming that there exists a virtual model M that describes a physical experiment E with a sufficient accuracy, in other words that

$$M \approx E, \tag{2}$$

$$\mathbf{y}^{\mathbf{E}} \approx \mathbf{y}^{\mathbf{M}} = M\left(\mathbf{x}^{\mathbf{M}}\right), \tag{3}$$

then it can be written that

$$\mathbf{y}^{\mathbf{E}} \approx M\left(\mathbf{x}^{\mathbf{M}}\right), \tag{4}$$

where $\mathbf{y}^{\mathbf{E}}$ and $\mathbf{y}^{\mathbf{M}}$ correspond to the experimental and simulation outputs (temperature distributions), respectively, and $\mathbf{x}^{\mathbf{M}}$ represents input parameters of the computational model, $\lambda_s(T)$ in particular. Eq. (4) can be used for the definition of the fitness function F to evaluate the quality of each candidate solution $\mathbf{x} = \mathbf{x}^{\mathbf{M}}$ as

$$F(\mathbf{x}) = \left\| \mathbf{y}^{\mathbf{E}} - M\left(\mathbf{x}^{\mathbf{M}}\right) \right\|. \tag{5}$$

As the root mean square error (RMSE) can be considered as a suitable method for the assessment of the difference between observations and predictions in computational modelling, Eq. (5) can be rewritten as

$$F(\mathbf{x}) = \sqrt{\sum_{i=1}^{n} \frac{\left(y_i^{\mathrm{E}} - y_i^{\mathrm{M}}\right)^2}{n}} \tag{6}$$

to define the fitness function in this research. In Eq. (6), y_1^{E}, y_2^{E}, …, y_n^{E} denote observed (experimental) values, while y_1^{M}, y_2^{M}, …, y_n^{M} represent predicted (simulated) values and n is the number of observations, i.e., values of temperature obtained for a given position at a given time. Here, unlike the traditional optimization techniques where higher means better, the lower value of fitness F indicates higher quality of the candidate. The best candidate is, therefore, that with $F(\mathbf{x}) = 0$. However, such a candidate exists only theoretically as there are noises due to measurement errors and/or model limitations and restrictions. Anyway, seeking for the lowest $F(\mathbf{x})$ determines the objective functions which can be expressed as minimization of the fitness function

$$\min F(\mathbf{x}) = \min \sqrt{\sum_{i=1}^{n} \frac{\left(y_i^{\mathrm{E}} - y_i^{\mathrm{M}}\right)^2}{n}}. \tag{7}$$

In the light of the aforementioned theory, each candidate solution $\mathbf{x}$ in this optimization problem is defined by a 6-dimensional vector that encodes the $\lambda_s(T)$ function. Each component of that vector represents a functional value (thermal conductivity) that needs to be combined with user-defined x-coordinate (temperature). These coordinates are given at the beginning of the optimization procedure to cover a desired temperature range and remain unchanged during the optimization procedure. In this way, six control points for each $\lambda_s(T)$ function are generated, while the last control point corresponds to the experimentally determined value of thermal conductivity of the sample at room temperature, $\lambda_{25} = 1.1617$ W m^{-1} K^{-1} (see Fig. 8). Before the computational simulation, each set of control points needs to be transformed to form a smooth and continuous $\lambda_s(T)$ function in the entire domain of definition (temperature range). Such preprocessing, i.e., transformation of $\mathbf{x}$ to $\lambda_s(T)$, is carried out mathematically using a piece-wise spline function outside the genetic algorithm, being motivated by achieving a reasonable compromise between computational time, convergence rate, and solution accuracy. The number of control points depends on available computational power, complexity of the mathematical model and size of the domain that is subject to the numerical approximation. As the number of optimized variables determines the size of population used in the genetic algorithm, i.e., the number of candidate solutions that interfere with each other and evolves during the optimization procedure, it is essential to find a reasonable representation of thermal conductivity vs. temperature function that will sufficiently describe the physical parameter with as low as possible requirements for the number of input variables. It is believed that six variables in a combination with one experimental value and the above mentioned transformation is adequate to find a solution with a reasonable accuracy.

Fig. 8. Experimental determination of thermal conductivity of the reference sample at room temperature using a transient heat pulse method.

The overall flowchart of the solution strategy is depicted in Fig. 9 for a better comprehensibility. The abbreviation GA used in the flowchart stands for the genetic algorithms.

3. Results and discussion

3.1. Calibration procedure

The objective of the calibration procedure was to demonstrate the ability of the atypical thermocouple set to measure temperature in a real-world application. Besides that, the gathered data were used to determine the conversion function of the K-type thermocouple set and to compare it against the standard data published by NIST [18]. The calibration procedure consisted of several steady state measurements for which the temperature vs. thermoelectric voltage function was plotted. For each steady state temperature, the average thermoelectric voltage from 12 thermocouple joints was calculated and the compensation of the cold junction was done. The thermoelectric voltage vs. temperature function obtained during the calibration procedure is shown in Fig. 10. Since the calibration was carried out for the temperature range between 50 and 200 °C only, the remaining data was extrapolated using a linear approximation. The voltage variations determined for the individual steady state temperatures and extrapolated data provided a background for an uncertainty analysis as well, being classified as an uncertainty of the type B. The highest difference was reached at 1100 °C, which corresponded to the maximum of the temperature range investigated, yielding a thermoelectric voltage difference of 1.39 mV. The relative calibration error was found to be lower than 3.2% T [K], which is a higher value than produced by standard K-type thermocouples, but such an agreement can be still considered as very good, enabling further thermocouple set applications.

3.2. Experimental results

The temperature field in the sample was monitored continuously

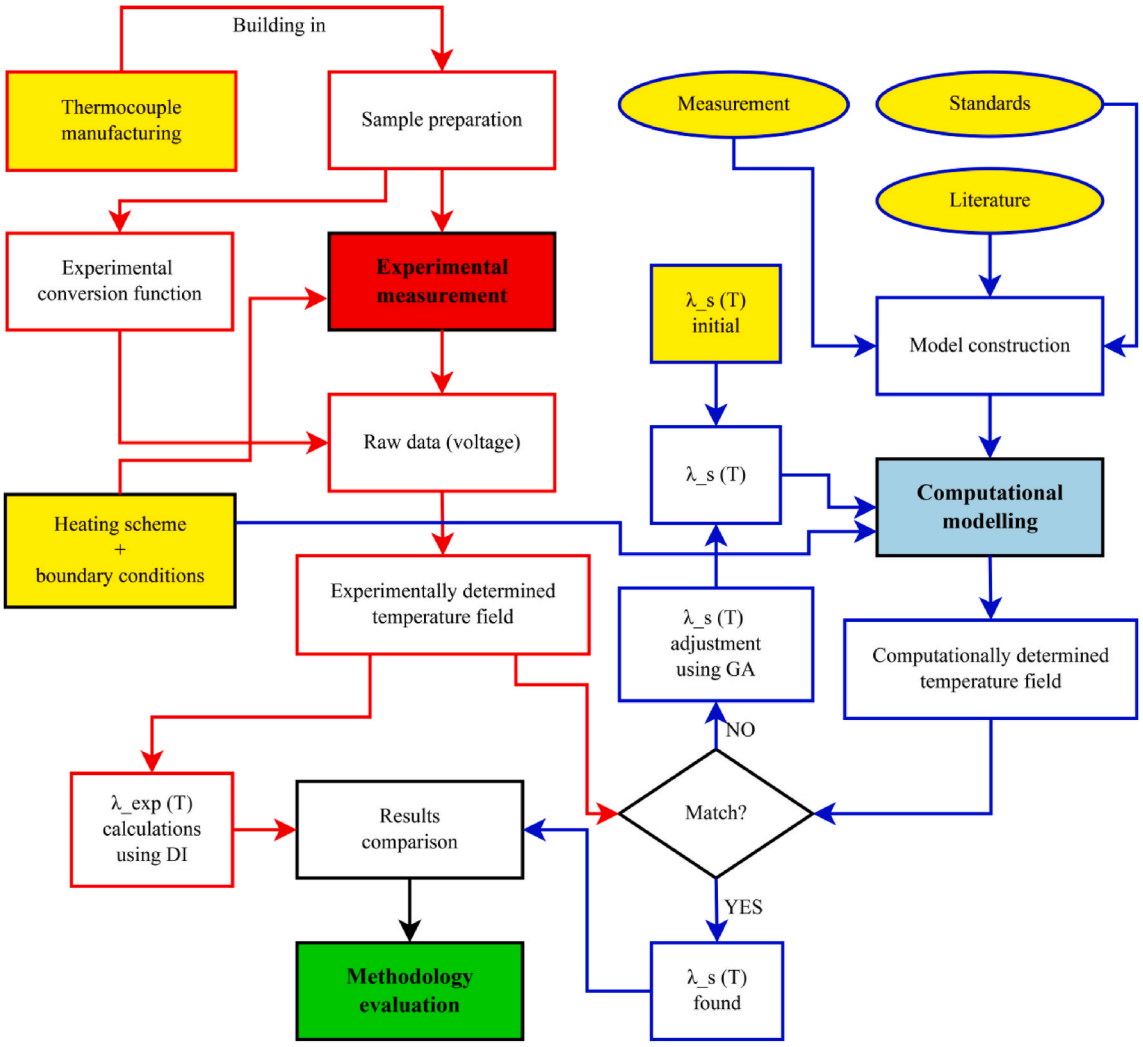

Fig. 9. The solution strategy.

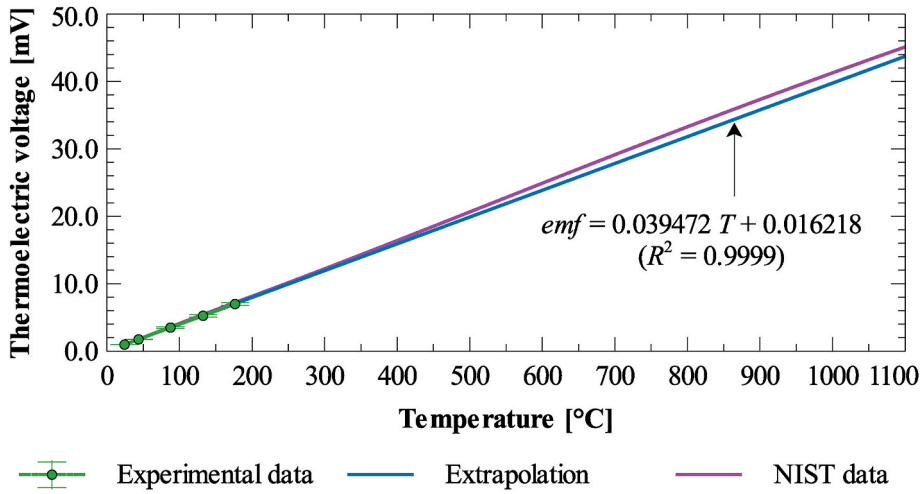

Fig. 10. The calibration procedure results including a comparison with NIST data.

every 10 s in twelve thermocouple joints in the sample as depicted in Fig. 4. The temperature distribution in four different times was then selected for further analysis, capturing the temperature increase gradually within the transient heat transfer mode. The last profile, recorded after 1200 s of heating, shows that the heat wave still did not reach the opposite side of the sample (see Fig. 11), which is an important assumption for the solution of the inverse heat conduction problem.

All the data measured are provided with the results of uncertainty

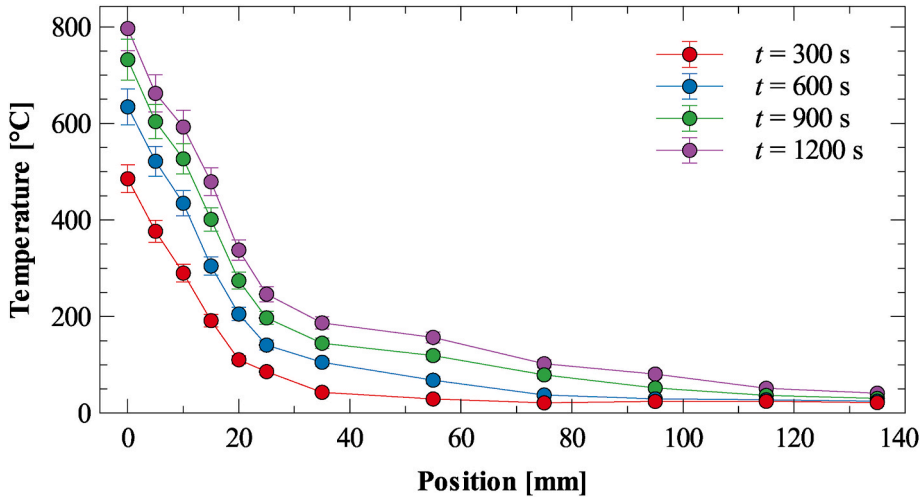

Fig. 11. Experimentally determined temperature distribution across the sample during the transient phase of the one sided heating experiment.

analysis combining the uncertainty of the type B (based on the deviations identified within the calibration procedure in Section 3.1) and of the type A, which was taken from the NIST dataset. The uncertainty found was then extended using a coverage factor, $k = 2$, to obtain a ~95% level of confidence. The average uncertainty was 8.9% which could be considered as an acceptable value for this kind of experiments and thus a starting point accurate enough for the subsequent computational modeling procedure.

3.3. Temperature distribution fitting

As it was mentioned in Section 2.3, dealing with the determination of the heat transfer coefficient on the sample's side in the furnace prior to the temperature distribution fitting is of a great importance; this coefficient has a direct impact on the amount of heat transferred to the sample and thus on the rate of heating. Since the mathematical model used for the temperature distribution modeling assumes the conductive mode only while the heat exchange in the sample-furnace system involves radiation and convection as well, a so-called effective value must be identified that considers all the aforementioned modes. To overcome this issue, a sensitivity analysis of the heat transfer coefficient was performed and the experimental and computational surface temperature evolutions were compared (Fig. 12).

It can be seen in Fig. 12, that the whole issue with the heat transfer coefficient is not as simple as it might look at the first glance. Since the radiative constituent of the coefficient is changing gradually with the change of the surface temperature, the coefficient is not constant [30, 31]. Obeying the generally known formula [32].

$$\alpha_f = \varepsilon\sigma\frac{\left(T_s^4 - T_{sur}^4\right)}{\left(T_s - T_{sur}\right)} = \varepsilon\sigma\left(T_s^2 + T_{sur}^2\right)\left(T_s + T_{sur}\right), \tag{8}$$

one can at least estimate a range of values that is possible to obtain to verify the correctness of this approach. In Eq. (8), ε [−] stands for the emissivity, $\sigma = 5.67 \times 10^{-8}$ W m^{-2} K^{-4} is the Stefan-Boltzmann constant, T_s [K] is the source temperature (heating wire) and T_{sur} [K] denotes the surface temperature. Assuming the emissivity of the sample surface being between 0.5 and 0.8 and the source temperature equal to the furnace set point ($T_s = 1373$ K), Eq. (8) yields α_f to be approximately in the range between 92 and 370 W m^{-2} K^{-1}. However, this equation has been derived for parallel plates which does not fully correspond to the furnace arrangement, where the heating wire is placed on the top of the chamber in a horizontal position, while the sample's surface is oriented vertically. Therefore, lower values of the heat transfer coefficient can be expected. A precise determination of the α_f coefficient would be probably a subject of a separate study, because it would be very demanding from the point of view of the extent of experimental work necessary.

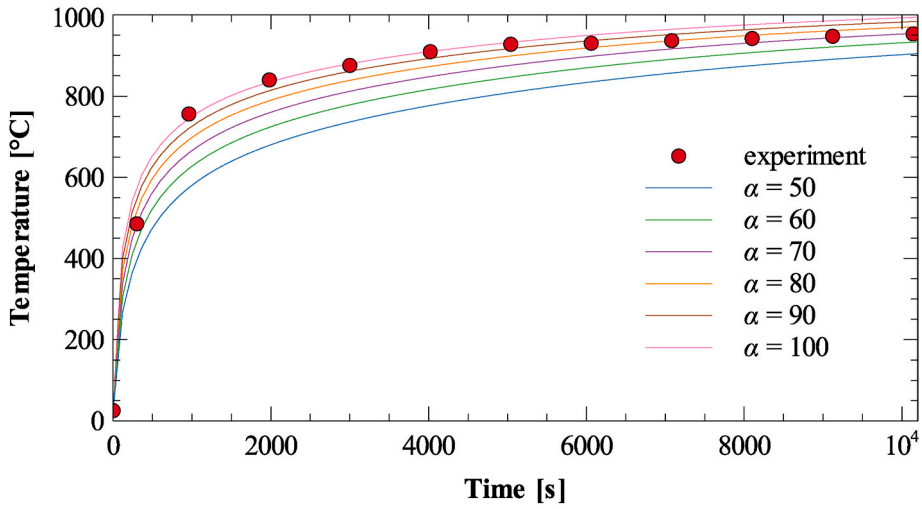

Fig. 12. Comparison of surface temperature evolution during the one sided heating experiment: experimental and computational results based on various values of the heat transfer coefficient.

Only a constant value was therefore selected for the modeling within this paper. Using the least square method based on a comparison of experimental and computational data obtained for $\alpha_f = \{50, 55, 60, \ldots, 90, 95, 100\}$, the highest agreement was achieved when $\alpha_f = 85$ W m^{-2} K^{-1} had been assumed, yielding the sum of squares equal to ~8556 K^2, which corresponded to an average temperature difference of 26.7 K (°C). Such a value of α_f is on the lower limit of the interval estimated before, but it conforms to the furnace arrangement.

A comparison of the heat transfer coefficient identified in this paper with other researchers' findings could be done only roughly, as most of the publications referring to this topic are based on unique or specific assumptions that are different than those used in the experimental setup in this paper. For instance, Shinoda et al. [33] or Yuan et al. [34] presented the radiative heat transfer coefficient only in standard temperature range related to domestic heating, being equal to ~5.0–6.0 W m^{-2} K^{-1}. On the other hand, Manara et al. [35] reported the heat transfer coefficient to be strongly increasing with temperature. Dealing with the temperatures up to 1100 °C, they assumed that the radiative heat transfer coefficient might be even higher than 500 W m^{-2} K^{-1}.

Using the genetic algorithms seeking procedure, the best solution, i.e., such a thermal conductivity of the sample, $\lambda_s(T)$, that in the interaction with the thermocouple set produces the same temperature distribution like that measured experimentally, was found in 2000 trials. The results of the seeking procedure are summarized in Fig. 13, showing the convergence history of the objective function. The thermal conductivity function, $\lambda_s(T)$, of the best solution found is shown in the same figure as well. The numerical approximation using a polynomial function of the third-degree is given in Eq. (9), yielding $R^2 = 0.9988$.

$$\lambda(T) = 1.569 \times 10^{-8} T^3 - 1.442 \times 10^{-5} T^2 - 3.802 \times 10^{-3} T + 0.6210 \quad (9)$$

The thermal conductivity function is completed by the results of the sensitivity analysis, expressing the results variance when limit values of the input parameters were assumed in the computational model. These values were quantified based on the measurement uncertainties evaluation and considering variance in the temperature field (±8.7%), thermal transport/storage parameters (chromel and alumel ± 1.5%, the sample ± 5.4%) and bulk density (chromel and alumel ± 1.5%, the sample ± 3.2%), and the heat transfer coefficient (±10.0%). The maximal variance of the thermal conductivity values reached 14.8%.

The convergence of the solution sought is obvious in Fig. 13a after ~1400 trials, which can be clearly demonstrated by a comparison of standard deviations of the trials 1–1400 (= 109570 K^2) and trials 1401–2000 (= 73704 K^2). The sporadic trials visible in Fig. 13a with disproportionally higher sum-of-square values correspond to random mutations that go along with the evolution algorithms seeking procedure. The best sum of squares calculated by means of the comparison of the experimentally and computationally obtained temperature distribution (see Fig. 14) reached 9009 K^2, which corresponded to an average temperature difference of 13.7 K(°C). Such an agreement could be considered satisfactory enough, especially when compared with the measurement uncertainties which were 22.7 °C in average.

One can notice in Fig. 14, that the computational profiles are smoother than those obtained experimentally as the computational model does not introduce any uncertainties and produces pure data. It means it is impossible to reach a 100% match between these two methods. The computational modeling must be therefore treated only as an approximation of the experimental results. Such an attitude can also be observed in other research studies [36].

3.4. Reduction of systematic errors

Once the thermal conductivity of the particular constituents of the sample-thermocouple system is identified, the thermal conductivity of the sample ($\lambda_s(T)$) in particular, the temperature field in the whole sample ($T(x,y,z,t)$) can be calculated. Adopting the same initial and boundary conditions as used in the experiment, the overall performance of the sample during the measurement procedure can be modeled. Since the model also enables to calculate the temperature field without the presence of the thermocouple, it makes it possible to predict such a temperature distribution which would not be affected by the systematic errors. Using a comparison with the experimentally obtained data $T(x,t)$, one can then quantify the effect of the thermocouple on the temperature field deformation. This quantification can be done under the assumption that $y = 0$ and $z = 0$ so that $T = T(x, 0, 0, t) = T(x, t)$, which limits the temperature field to the thermocouple core wire similarly like in the real experiment. The comparison is depicted in Fig. 15a, capturing the temperature evolution in the twelve points corresponding to the positions of the thermocouples. The solid lines in Fig. 15a denote the temperature evolution in the sample with the built-in thermocouple set, while the dotted lines show the temperature evolution when the thermocouple set presence is computationally compensated. One can notice, that the presence of thermocouples can affect the temperatures recorded by up to 64 °C, especially in case of positions located close to the heated surface. This happens due to the thermal conductivity of metals embedded in the sample, that conduct the heat much faster than the porous body. Therefore, the temperature increase should be in fact higher than recorded, which can be confirmed by comparing the temperature profiles in the positions of 0, 5, 10 and 15 mm. On the other hand, the deeper positions are affected by the heat transferred from the heated surface via the metal wires, so their temperature is increasing

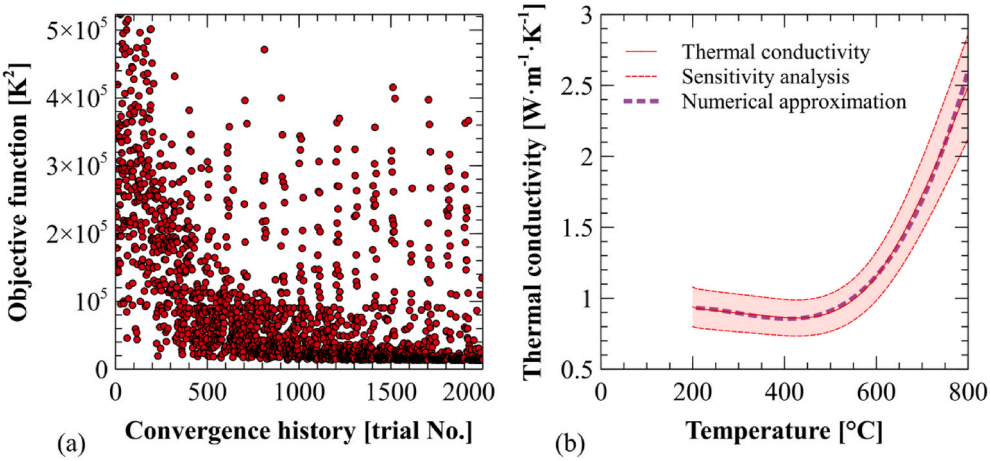

Fig. 13. Description of the genetic algorithms seeking procedure: (a) convergence history and (b) the thermal conductivity function $\lambda_s(T)$ corresponding to the best solution found.

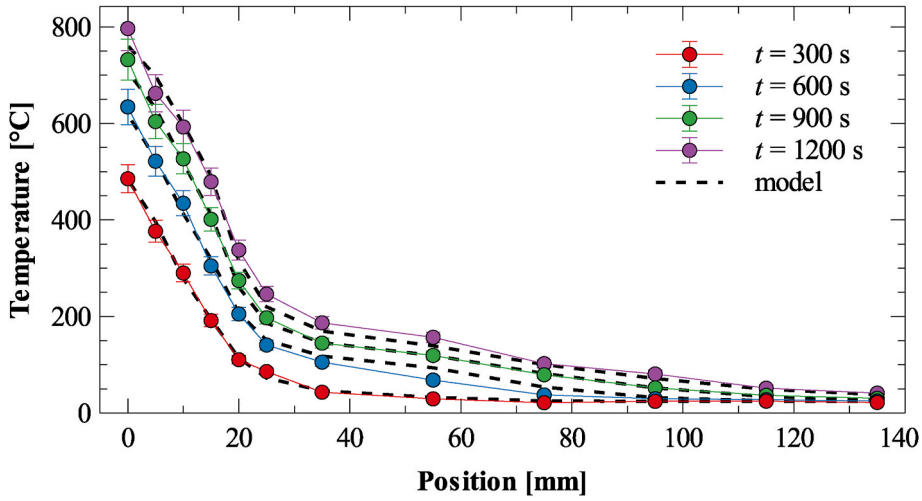

Fig. 14. Comparison of experimentally and computationally obtained temperature distribution in the sample during the one-sided heating experiment.

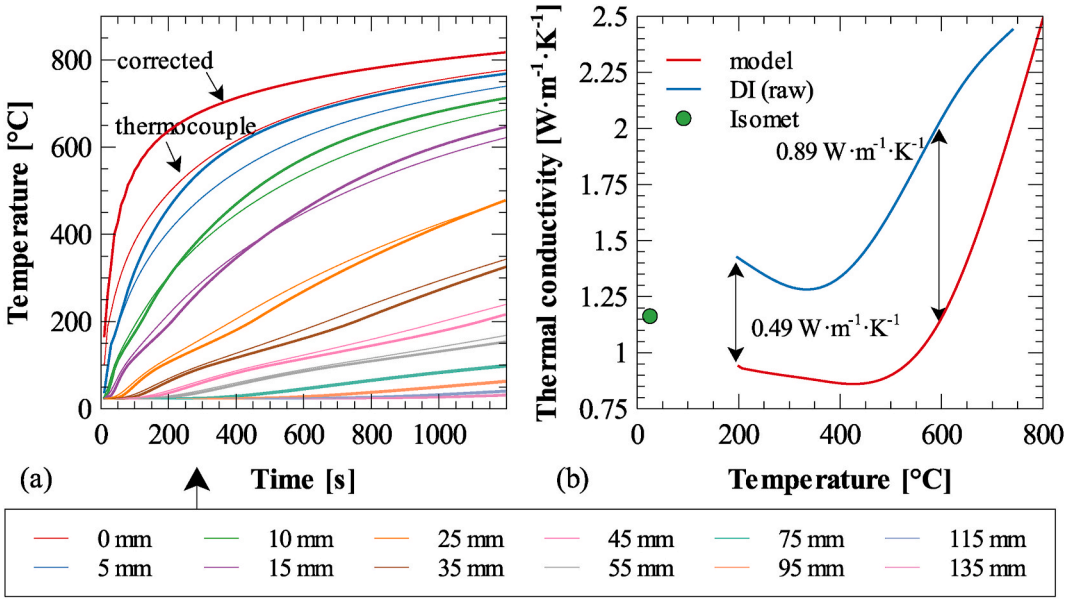

Fig. 15. (a) Comparison of the temperature evolution in the sample with and without the thermocouple set, (b) comparison of thermal conductivity determined by different methods.

faster. This is obvious when the profiles in the positions of 25, 35, 45 and 55 mm are analyzed. In case of the remaining profiles (75, 95, 115 and 135 mm) only small differences were detected, as they were not subject of any substantial temperature changes within the first 1200 s of heating.

Even if the temperature differences were observed for only a short period of time and were restricted mostly to the depth of ~50 mm, the further processing of the data measured could be still negatively affected. Determination of thermal conductivity, $\lambda_{exp}(T)$, based on the double integration (DI) method using the original experimental temperature data [10] is a typical example in that respect. Such a thermal conductivity function is depicted in Fig. 15b (labeled as DI (raw)), being compared with the solution found by the computational modeling approach ($\lambda_s(T)$) and with the transient heat pulse method. Both thermal conductivity functions, $\lambda_{exp}(T)$ and ($\lambda_s(T)$, were obtained using the $\rho(T)$ and $c_p(T)$ values as depicted in Fig. 7. Apparently, the processing of the raw data provided higher thermal conductivity as it neglected the thermocouple presence and the temperature field deformation that corresponded to a faster heat transfer. The difference at 200 °C was found to be 0.491 W m^{-1} K^{-1}, but it reached up to 0.889 W m^{-1} K^{-1} at 605 °C as demonstrated in Fig. 15b. It means, the relative systematic errors accompanying the experimental measurement might represent up to 46.1% of the measured value.

Fig. 16 shows a comparison of the thermal conductivity found by the modeling procedure with those reported by other researchers. Unfortunately, an exact comparison could not be done as other results reported in the literature are related to a different sample composition or to a different temperature range. Therefore, high alumina cement based materials relatively similar to the high alumina cement mortar analyzed in this paper were selected for this purpose.

Espinoza-Paredes et al. [12] reported the thermal conductivity of geothermal cementing systems to be between 0.67 and 0.75 W m^{-1} K^{-1} between 28 and 220 °C. Their values are lower than those reported in this paper, but one must consider a different sample preparation procedure and composition. Ruh and Renkey [37] studied refractory castables made of high-alumina cement. Their results, ~1.05 W m^{-1} K^{-1} in average between 320 and 800 °C, are very similar to those reported in this paper, but the thermal history was mentioned as an factor affecting

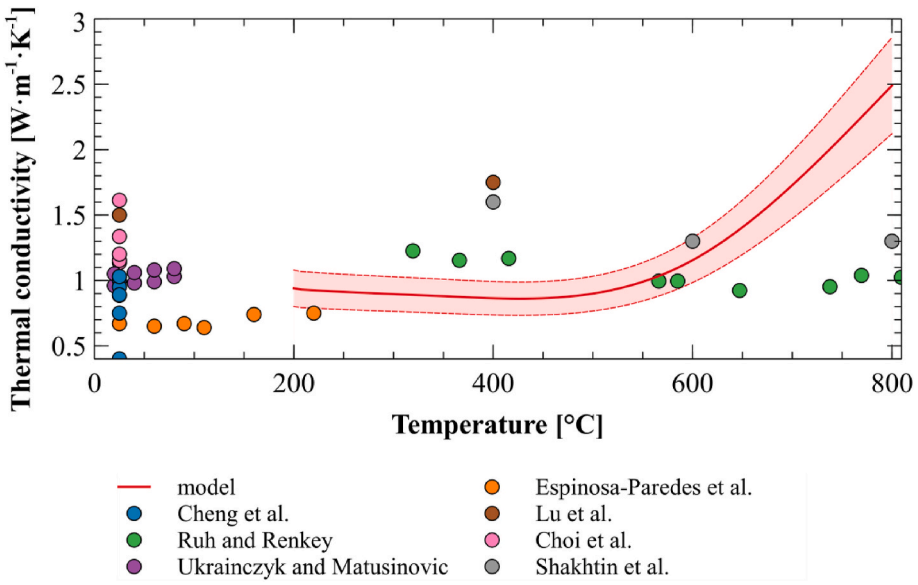

Fig. 16. Comparison of thermal conductivity of high alumina cement based materials reported in the literature.

the results. Lu et al. [38] reported higher thermal conductivity of their samples with higher amount of alumina due to an addition of metakaolin. However, the thermal conductivity of 1.75 W m^{-1} K^{-1} at 400 °C can be ascribed to a higher density and lower porosity as they intended to produce a high performance concrete. Shakhtin et al. [39] reported the thermal conductivity of mullite-corundum refractories with Al_2O_3 content of ~78% to be 1.30 W m^{-1} K^{-1} between 600 and 800 °C, which is a very good agreement with our results. Choi et al. [40] investigated alumina cementitious materials, reporting their thermal conductivity to be 0.89–1.33 W m^{-1} K^{-1} at 25 °C. Unfortunately, the dependence of the thermal conductivity on temperature was not reported. Similarly, dealing with thermal properties of aluminate cement paste with blast furnace slag, Cheng et al. [41] reported its thermal conductivity at room temperature to be between 0.40 and 1.03 W m^{-1} K^{-1}, depending on a treatment temperature. Ukrainczyk and Matusinovic [42] studied thermal properties of hydrating calcium aluminate cement pastes. In the temperature range of 20 and 80 °C, they reported the thermal conductivity to be 0.96–1.09 W m^{-1} K^{-1}, which is also very similar to the results found within this paper.

Based on the above mentioned, one can conclude that the computational technique presented in this paper is able to reduce the systematic errors accompanying non-equilibrium thermocouple measurements and make the thermocouple applications more reliable. This can be considered as its main added value, as compared with the experiments performed in a common way.

4. Conclusions

The utilization of thermocouples for determination of thermal properties or monitoring thermal performance of building materials is quite common nowadays. However, a higher number of thermocouples in a sample, e.g., in case of a non-equilibrium temperature field determination, goes along with systematic errors due to much higher thermal conductivity of metals than that of a porous body. This phenomenon was considered as a serious drawback of using thermocouple systems in the field of building materials engineering so far. Therefore, in this paper a method based on computational modeling of heat transfer was introduced to overcome this problem and to provide an added value for thermocouple measurements.

The practical applicability of the method was demonstrated on an experimental investigation of a high-alumina cement mortar, which underwent a one-sided heating. The temperature field recorded during a transient heat transfer mode was subsequently analyzed to determine the thermal conductivity as a function of temperature. The computational model, representing an exact replica of the experiment, was then used to find such a thermal conductivity of the sample, that produced the same outputs as the real experiment. Since the model treats the thermal conductivity for all components of the sample-thermocouple system separately, the found solution related solely to the material of the sample can be considered as more accurate, being less affected by the systematic errors that are related to the presence of the thermocouple. It was found that the distortion of the temperature field might reach up to 64 °C which, after further processing, significantly affected the thermal conductivity calculated. The differences in the thermal conductivity functions were highest at 605 °C, accounting for 0.889 W m^{-1} K^{-1}. Comparing the experimental and computational results it can be concluded, that the computational modeling contributed substantially to the reduction of systematic errors, which originally accounted for up to 46.1%. It is important to note that such a high value reflected the non-standard experimental setup used. Possible discrepancies between physical and mathematical models due to some simplifications adopted could also affect the obtained results.

Declaration of competing interest

The authors declare that they have no known competing financial interests or personal relationships that could have appeared to influence the work reported in this paper.

Acknowledgment

This research has been supported by the Czech Science Foundation, under project No. 20-00653S.

References

[1] L.B. Hunt, The early history of the thermocouple, Platin. Met. Rev. 8 (1) (1964) 23–28.
[2] S.K. Singh, M.K. Yadav, R. Sonawane, S. Khandekar, K. Muralidhar, Estimation of time-dependent wall heat flux from single thermocouple data, Int. J. Therm. Sci. 115 (2017) 1–15.
[3] M.K. Yadav, S.K. Singh, A. Parwez, S. Khandekar, Inverse models for transient wall heat flux estimation based on single and multi-point temperature measurements, Int. J. Therm. Sci. 124 (2018) 307–317.
[4] A.A.A. Al-Naghi, M.K. Rahman, O.S.B. Al-Amoudi, S.U. Al-Dulaijan, Thermal performance evaluation of walls with AAC blocks, insulating plaster, and reflective coating, J. Energy Eng. 146 (2) (2020).

[5] H. Ding, Y. Guo, Z. Wang, Study on laser irradiation temperature field of carbon fiber reinforced plastic composites, Mater. Res. Express 7 (3) (2020).
[6] M. Bendouma, T. Colinart, P. Glouannec, H. Noel, Laboratory study on hygrothermal behavior of three external thermal insulation systems, Energy Build. 210 (2020).
[7] K. Drozdzol, Experimental fire testing of an innovative three-layer chimney for residential buildings, Journal of Building Engineering 28 (2020).
[8] C. Lou, W.H. Li, H.C. Zhou, C.T. Salinas, Experimental investigation on simultaneous measurement of temperature distributions and radiative properties in an oil-fired tunnel furnace by radiation analysis, Int. J. Heat Mass Tran. 54 (1–3) (2011) 1–8.
[9] T. Arends, A.J. Barakat, L. Pel, Moisture transport in pine wood during one-sided heating studied by NMR, Exp. Therm. Fluid Sci. 99 (2018) 259–271.
[10] R. Cerny, E. Vejmelkova, Apparent thermal conductivity approach at high-temperature measurements of porous materials, Measurement 44 (7) (2011) 1220–1228.
[11] T. Fischedick, M. Kind, B. Dietrich, Radial two-phase thermal conductivity of ceramic sponges up to high temperatures – experimental results and correlations, Int. J. Therm. Sci. 114 (2017) 98–113.
[12] G. Espinosa-Paredes, A. Garcia, E. Santoyo, E. Contreras, J.M. Morales, Thermal property measurement of Mexican geothermal cementing systems using an experimental technique based on the Jaeger method, Appl. Therm. Eng. 22 (3) (2002) 279–294.
[13] V.V. Cherepanov, O.M. Alifanov, A.V. Morzhukhina, S.A. Budnik, Highly porous thermal protection materials: modelling and prediction of the methodical experimental errors, Acta Astronaut. 128 (2016) 392–400.
[14] Q. Kong, G.S. Jiang, Y.C. Liu, M. Yu, Numerical and experimental study on temperature field reconstruction based on acoustic tomography, Appl. Therm. Eng. 170 (2020) 13.
[15] I. Ihara, M. Takahashi, A new method for internal temperature profile measurement by ultrasound, in: 2007 IEEE Instrumentation & Measurement Technology Conference IMTC 2007, 2007, pp. 1–5.
[16] S. Wen, H. Qi, Z.T. Niu, L.Y. Wei, Y.T. Ren, Efficient and robust prediction of internal temperature distribution and boundary heat flux in participating media by using the Kalman smoothing technique, Int. J. Heat Mass Tran. 147 (2020) 14.
[17] M. Nabil, J.M. Khodadadi, Computational/analytical study of the transient hot wire-based thermal conductivity measurements near phase transition, Int. J. Heat Mass Tran. 111 (2017) 895–907.
[18] K.M. Garrity, D.C. Ripple, M. Araya, C.R. Cabrera, L.C. Murillo, M.E. de Vanegas, D. J. Gee, E. Guillen, S. Martinez-Martinez, E. Mendez-Lango, L. Mussio, S. G. Petkovic, K.N. Quelhas, G. Rangugni, O. Robatto, E.V. Rocha, A regional comparison of calibration results for type K thermocouple wire from (100 to 1,100) degrees C, Int. J. Thermophys. 29 (5) (2008) 1828–1837.
[19] G.W. Burns, M.G. Scroger, G.F. Strouse, M.C. Croarkin, W.F. Guthrie, Temperature-Electromotive Force Reference Functions and Tables for the Letter-Designated Thermocouple Types Based on the ITS-90, U.S. Department of Commerce, National Institute of Standards and Technology, 1993.
[20] V. Koci, J. Koci, T. Korecky, J. Madera, R. Cerny, Determination of radiative heat transfer coefficient at high temperatures using a combined experimental-computational technique, Meas. Sci. Rev. 15 (2) (2015) 85–91.
[21] B. Sundqvist, Thermal diffusivity and thermal conductivity of Chromel, Alumel, and Constantan in the range 100–450 K, J. Appl. Phys. 72 (2) (1992) 539–545.
[22] J.H. Holland, Outline for a logical theory of adaptive systems, J. ACM 9 (3) (1962) 297–314.
[23] X. Mao, J. Wang, C. Yuan, W. Yu, J. Gan, A dynamic traffic assignment model for the sustainability of pavement performance, Sustainability 11 (1) (2019).
[24] G.S. Wang, Y.R. Li, F.K. Huang, Parametric identification and damage assessment of real buildings, in: R. Caspeele, L. Taerwe, D.M. Frangopol (Eds.), Life Cycle Analysis and Assessment in Civil Engineering: towards an Integrated Vision. Proceedings of the Sixth International Symposium on Life-Cycle Civil Engineering (IALCCE 2018), 28-31 October 2018, Ghent, Belgium, CRC Press, 2019, pp. 602–614.
[25] V. Koci, J. Koci, J. Madera, R. Cerny, Assessment of fast heat evolving processes using inverse analysis of calorimetric data, Int. J. Heat Mass Tran. 115 (2017) 831–838.
[26] A. Muc, Evolutionary design of engineering constructions, Lat. Am. J. Solid. Struct. 15 (4) (2018).
[27] GRADE Algorithm, 2009 available online at: http://mech.fsv.cvut.cz/~anicka/grade/grade.html#pub. accessed April 12, 2021.
[28] A. Ibrahimbegović, C. Knopf-Lenoir, A. Kučerová, P. Villon, Optimal design and optimal control of structures undergoing finite rotations and elastic deformations, Int. J. Numer. Methods Eng. 61 (14) (2004) 2428–2460.
[29] A. Kučerová, M. Lepš, J. Zeman, Back analysis of microplane model parameters using soft computing methods, Comput. Assist. Mech. Eng. Sci.: Comput. Assist. Mech. Eng. Sci. 14 (2) (2007) 219–242.
[30] H. Louahlia, P. Panday, E.A. Artioukhine, Inverse determination of the local heat transfer coefficients for nucleate boiling on a horizontal cylinder, Journal of Heat Transfer-Transactions of the ASME 125 (2003).
[31] K. Cao, D. Lesnic, J. Liu, Simultaneous reconstruction of space-dependent heat transfer coefficients and initial temperature, J. Comput. Appl. Math. 375 (2020) 112800.
[32] T.L. Bergman, A.S. Lavine, F.P. Incropera, D.P. Dewitt, Fundamentals of Heat and Mass Transfer, seventh ed., Wiley, Hoboken, NJ, 2011.
[33] J. Shinoda, O. Kazanci, S.-i. Tanabe, B.W. Olesen, Review on the Surface Heat Transfer Coefficients of Radiant Systems, 2019.
[34] Y. Yuan, X. Zhang, X. Zhou, Simplified correlations for heat transfer coefficient and heat flux density of radiant ceiling panels, Science and Technology for the Built Environment 23 (2017), 00-00.
[35] J. Manara, M. Arduini-Schuster, H.J. Rätzer-Scheibe, U. Schulz, Infrared-optical properties and heat transfer coefficients of semitransparent thermal barrier coatings, Surf. Coating. Technol. 203 (8) (2009) 1059–1068.
[36] R. Anderson, L. Bates, E. Johnson, J.F. Morris, Packed bed thermal energy storage: a simplified experimentally validated model, Journal of Energy Storage 4 (2015) 14–23.
[37] E. Ruh, A.L. Renkey, Thermal conductivity of refractory castables, J. Am. Ceram. Soc. 46 (2) (1963) 92.
[38] D. Lu, Z. Tang, L. Zhang, J. Zhou, Y. Gong, Y. Tian, J. Zhong, Effects of combined usage of supplementary cementitious materials on the thermal properties and microstructure of high-performance concrete at high temperatures, Materials 13 (8) (2020).
[39] D.M. Shakhtin, V.I. Pechenezhskii, A.G. Karaulov, N.M. Kvasman, V. P. Kravchenko, Kabakova II, V.A. Ustichenko, G.E. Kalita, G.N. Shcherbenko, L. M. Yakobchuk, Thermal-conductivity of corundum, high-alumina, magnesia, zirconium, and chromate refractories in the 400-1800-degrees-C range, Refractories 23 (5–6) (1982) 223–227.
[40] Y.C. Choi, I.H. Yang, J.H. Lee, Thermal and mechanical properties of alumina cementitious composite materials, Journal of the Korean Recycled Construction Resources Institute 3 (3) (2015) 199–205.
[41] X. Cheng, Q. Dong, Y. Ma, C. Zhang, X. Gao, Y. Yu, Z. Wen, C. Zhang, X. Guo, Mechanical and thermal properties of aluminate cement paste with blast furnace slag at high temperatures, Construct. Build. Mater. (2019) 228.
[42] N. Ukraincyk, T. Matusinovic, Thermal properties of hydrating calcium aluminate cement pastes, Cement Concr. Res. 40 (1) (2010) 128–136.